Renewable and Sustainable Energy Reviews 104 (2019) 281–295

Contents lists available at ScienceDirect

Renewable and Sustainable Energy Reviews

journal homepage: www.elsevier.com/locate/rser

# Significant wave height forecasting *via* an extreme learning machine model integrated with improved complete ensemble empirical mode decomposition

Mumtaz Ali[a], Ramendra Prasad[a,b,*]

[a] School of Agricultural, Computational, and Environmental Sciences, Institute of Agriculture and Environment, University of Southern Queensland, Springfield, QLD 4300, Australia

[b] Department of Science, School of Science and Technology, The University of Fiji, Saweni, Lautoka, Fiji

ARTICLE INFO

*Keywords:*
ELM
OSELM
RF
ICEEMDAN
Coastal waves
Forecast

ABSTRACT

Data-intelligent algorithms designed for forecasting significant height of coastal waves over the relatively short time period in coastal zones can generate crucial information about enhancing the renewable energy production. In this study, a machine learning model is designed and evaluated for forecasting significant wave height (Hs) within the eastern coastal zones of Australia. The extreme learning machine (ELM) model is coupled with an improved complete ensemble empirical mode decomposition method with adaptive noise (ICEEMDAN) to design the proposed ICEEMDAN-ELM model. This model incorporates the historical lagged series of Hs as the model's predictor to forecast future Hs. The ICEEMDAN algorithm demarcates the original Hs data from January-2000 to March-2018, recorded at 30-min intervals, into decomposed signals *i.e.*, intrinsic mode functions (IMFs) and a residual component. After decomposition, the partial autocorrelation function is determined for each IMF and the residual sub-series to determine the statistically significant lagged input dataset. The ELM model is applied for forecasting of each IMF by incorporating the significant antecedent Hs sub-series as inputs. Finally, all the forecasted IMFs are summed up to obtain the final forecasted Hs. The results are benchmarked with those from an online sequential extreme learning machine (OSELM) and random forest (RF) integrated with ICEEMDAN, *i.e.*, the ICEEMDAN-OSELM and ICEEMDAN-RF models. The proposed ICEEMDAN-ELM model is tested geographically at two coastal sites of the Queensland state, Australia. The testing performance of all the standalone (ELM, OSELM, RF) and integrated models (ICEEMDAN-ELM, ICEEMDAN-OSELM, ICEEMDAN-RF), according to robust statistical error metrics, is satisfactory; however, the hybrid ICEEMDAN-ELM model is found to be a beneficial Hs forecasting tool in accordance to high performance accuracy. The proposed ICEEMDAN-ELM model can be considered as a pertinent decision-support framework and is vital for designing of reliable ocean energy converters.

## 1. Introduction

Rising carbon dioxide levels with a subsequent increase in global mean temperatures compounded by rapidly depleting non-renewable energy sources have pushed for advancements in environmental-friendly and renewable energy technologies. The technologies for hydro-electricity, solar and wind energy are well established and reasonably economical, yet the developments in ocean renewable energy have been lagging behind [1]. Australia, the 'island-continent' is surrounded by a vast ocean with enormous wave energy potential. The key advantage of Australia is that huge wave energy resources are within viable proximity to household and prospective industries [2] that can allow for the cost-effective transmission of electricity. In addition, the wave energy is found to have a higher degree of certainty and consistency in comparison to wind energy [2]. However, wave is a variable source of energy controlled by nature's chaotic behavior. Therefore, this intermittency component must carefully be studied through appropriate forecasting approaches in order to gauge the availability and reliability of wave energy for sustainable electricity generation.

One key ocean wave parameter that needs to be forecasted is the significant wave height (Hs). Since Hs describes the ocean wave conditions, very short-term Hs forecasts are imperative for electricity generation [3], oceanic engineering purposes, improvement of safety and efficiency in maritime activities [4] and coastal disaster risk management. The wave power level is directly associated with Hs, and it is the key parameter in wave energy generation [5]. Hence, scholars

* Corresponding author at: Department of Science, School of Science and Technology, The University of Fiji, Saweni, Lautoka, Fiji.
*E-mail addresses:* Mumtaz.Alli@usq.edu.au (M. Ali), ramendrap@unifiji.ac.fj (R. Prasad).

https://doi.org/10.1016/j.rser.2019.01.014
Received 12 July 2018; Received in revised form 3 December 2018; Accepted 5 January 2019
Available online 22 January 2019
1364-0321/ © 2019 Elsevier Ltd. All rights reserved.

have developed a number of forecasting models using data-intelligent approaches in order to emulate Hs, yet these studies are still in their nascent stages. The algorithms that have been explored in prediction of ocean wave parameters includes classification and regression tree type C5 algorithm [6], M5' tree models [7], artificial neural networks (ANN) [6,8,9], support vector machine (SVM) [8,9], Adaptive-Network-Based Fuzzy Inference System (ANFIS) [9,10]. In a review on computational intelligence in wave energy applications, Cuadra, Salcedo-Sanz [11] found that ANN was a widely used model with better performance in comparison to regression models. However, these are classical standalone models, which may not be able to sufficiently capture the non-linear dynamics of the stochastic ocean waves.

The natural stochastic nature of the ocean waves that induces non-stationarity and non-linearity within the time series is one of the most important challenges in coastal and maritime engineering applications [6] and forecasting. The non-stationarity features bring about non-normality, bimodality, asymmetric cycles and non-linearities embedded within the series. In order to handle non-stationarity features, the inputs for respective data-driven models need to be properly pre-processed [12–15]. Therefore, a multi-resolution analysis (MRA) [16,17] tool is utilized to unveil the embedded features overcoming the non-stationarity issue.

Conventionally, the Fourier transformation was used, yet it only performs transformation at frequency resolutions and loses the more important time stamp. The discrete wavelet transformation (DWT) which is an alternative MRA utility has been widely used in many forecasting applications [18–21]. Similarly, few studies with discrete wavelet hybrid models have been applied in Hs forecasting whereby the widely used ANN has been hybridized with DWT called W-ANN [22–25]. In another study, Özger [26] performed a study with wavelet fuzzy logic approach. The DWT, however, has a critical weakness called the decimation effect. During frequency resolution conversions of DWT, only half the wavelet coefficients are generated and the other half is recursively transformed at a coarser resolution leading to a loss of vital information [27]. As a result, a non-decimated wavelet tool called the maximum-overlap discrete wavelet transformation (MODWT) ideally overcomes the decimation issue [27–31]. Yet, MODWT has not been explored in Hs forecasting purposes. The other issue with wavelets (including DWT and MODWT) is that they require the defining of a well-suited mother wavelet *a priori* [32]. This is still an unresolved issue and generally requires a lengthy trial and error process [28]. On the other hand, the empirical mode decomposition (EMD) multiresolution utility developed by Huang et al., [33] offers self-adaptability by avoiding the need for any basis function and/or mother wavelets. EMD is completely data-adaptive that uses temporal local decomposition method in extracting the salient features. Then EMD isolates these significant features into sub-series that represents the physical structure of the time series [34]. Consequently, EMD based models have been adopted in forecasting Hs including EMD-Autoregressive (AR) model [4] and EMD-support vector regression (SVR) [35]. However, the performance of EMD is compromised by the inherent 'mode mixing' shortcoming. The ensemble-EMD (EEMD) solves this issue by addition of a Gaussian white noise to the original (undecomposed) time series and then extracts the embedded periodic and trend information [36]. However, the reconstruction of EEMD decomposed data is not completely noise-free as a different number of IMFs can be obtained [37]. Hence, to create a completely noise-free reconstruction of data, a complete ensemble empirical mode decomposition with adaptive noise (CEEMDAN) was proposed [37]. CEEMDAN requires a Gaussian white noise to be added sequentially at each decomposition stage, yet has limitations on parallel computing resulting in slower performance than EEMD [38]. The newer, improved complete ensemble empirical mode decomposition with adaptive noise (ICEEMDAN) was developed in response to address the shortcomings of the predecessor EMD-based algorithms [38].

The ICEEMDAN has successfully been explored for multi-resolution signal processing, particularly in vibrational fault diagnosis [39,40]. ICEEMDAN has also been successfully applied in the estimation of decay ratio in boiling water reactors [41] and to reconstruct spectral data for removing noise form near-infrared spectra signals [42]. Studies pertaining to modeling showed improved performance of ICEEMDAN integrated with particle swarm optimization (PSO) of SVR (ICEEMDAN-PSO-SVR) in the modeling of near-infrared non-invasive glucose detection [43]. In a recent study, Al-Musaylh et al., [44] applied ICEEMDAN-PSO-SVR in long-term electrical energy demand predictions. These studies found that ICEEMDAN hybridized models performed better in emulating the respective variables capturing the non-stationarity features well [43,44]. To the best of the authors' knowledge, the application of ICEEMDAN multi-resolution technique is yet to be explored in forecasting of Hs.

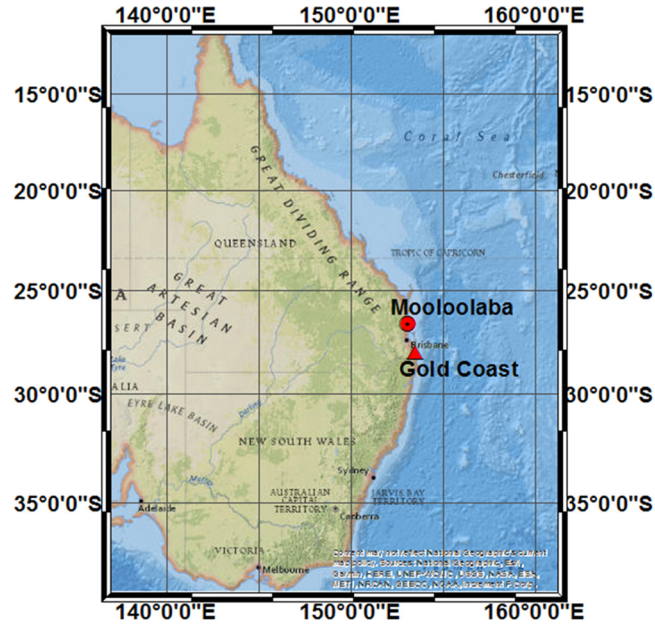


**Fig. 1.** Map of the study region showing the locations of the off-shore floating buoys.

The aim of the paper is to address non-stationarity issues in Hs forecasting at a very short-time *i.e.*, half-hourly forecast horizons using a non-decimated, self-adaptive, fast and computationally efficient data pre-processing utility (ICEEMDAN). Subsequently, the ICEEMDAN is integrated with a fast and efficient extreme learning algorithm (ELM) to develop the novel ICEEMDAN-ELM models in Hs forecasting. Two sites at the eastern coast of Australia that have great wave energy generation potential have been selected to validate the models. The ICEEMDAN-ELM is benchmarked against a comparative online sequential ELM (ICEEMDAN-OSELM) and random forest (ICEEMDAN-RF) and the respective standalone models. The application of ELM and their variants are very uncommon in Hs forecasting studies as only two studies have been noted that used ensemble-ELM [45] and grouping genetic algorithm-ELM [46]. Also, no such studies with random forest have been performed so far which is substantiated here.

## 2. Theoretical framework

The basic theory involved in the construction of the proposed collaborative ICEEMDAN-ELM model for Hs forecasting is presented in this section.

### 2.1. Improved complete ensemble empirical mode decomposition with adaptive noise (ICEEMDAN) model

The empirical mode decomposition EMD [47] is a data intelligent model to analyze the nonlinear and non-stationary data. The EMD algorithm splits the time series data, Hs($t$), into resolved components or intrinsic mode functions (IMFs) and a residual component. The improved version of EMD known as ICEEMDAN [38] decomposes the data Hs($t$) into several IMFs with an additional residual factor in the

**Table 1**
Geographic locations and statistical characteristics of significant wave height at the selected sites.

| Station names | Location | | Statistical features of half-hourly significant wave height (m) | | | | |
|---|---|---|---|---|---|---|---|
| | Long. (°E) | Lat. (°S) | Min. | Max. | Mean | Skewness | Kurtosis |
| Gold Coast | 153.4000° | 28.0167° | 0.18 | 6.27 | 1.12 | 1.81 | 6.52 |
| Mooloolaba | 53.1180° | 26.6820° | 0.04 | 5.89 | 1.19 | 1.38 | 3.56 |

following way:

1. First, the EMD algorithm with an operator $\lambda_j(.)$ at $j^{th}$ mode decomposes Hs($t$) whereas another operator $\tau(.)$ generates the local mean of Hs($t$).
2. Further, with $\eta_i$ as the Gaussian white noise with variance ranging from 0 to 1, the EMD algorithm first computes the local means of $n$ realizations ($\mathrm{Hs_i}(t)$) as follows:

   $$\mathrm{Hs_i}(t) = \mathrm{Hs}(t) + \alpha_0\lambda_1(\eta_i(t))$$

   where $\alpha_0 = \phi_0 \mathrm{std(Hs)}/\mathrm{std}(\lambda_1(\eta_i(t)))$ is incorporated at the initial stage to remove the fraction of noise energy. The term $\phi_0$ is the reciprocal of the desired signal to noise ratio (SNR) between the first added noise and the analyzed signal [38] and 'std' is the standard deviation.
3. The remaining component after determining the local means is the first residual component ($\gamma_1$) denoted as $\gamma_1(t) = \langle\tau(\mathrm{Hs_i}(t))\rangle$.
4. The computed first IMF at $j = 1$ is $\mathrm{IMF_1}(t) = \mathrm{Hs}(t) - \gamma_1(t)$.
5. Consequently, the second residue, $\gamma_2(t)$, is the average of the local means $\gamma_1(t) + \alpha_1\lambda_1(\eta_i(t))$ which can be mathematically represented as; $\mathrm{IMF_2}(t) = \gamma_1(t) - \gamma_2(t) = \gamma_1(t) - \langle\tau(\gamma_1(t) + \alpha_1\lambda_2(\eta_i(t)))\rangle$ where $\alpha_1 = \phi_1\mathrm{std(Hs)}/\mathrm{std}(\lambda_2(\eta_i(t)))$. The third residue is given as $\gamma_3(t) = \langle\tau(\gamma_2(t)+\alpha_2\lambda_3(\eta_i(t)))\rangle$, where $\alpha_2 = \phi_2\mathrm{std(Hs)}/\mathrm{std}(\lambda_3(\eta_i(t)))$ and $\mathrm{IMF_3}(t) = \gamma_2(t)-\gamma_3(t)$.
6. The residue and mode for $j = 3, 4, ...,J$ at $j^{th}$ stance can be computed as
   $\gamma_j(t) = \langle\tau(\gamma_{j-1}(t)+\alpha_{j-1}\lambda_j(\eta_i(t)))\rangle$ where $\alpha_{j-1} = \phi_1\mathrm{std(Hs)}/\mathrm{std}(\lambda_j(\eta_i(t)))$.

   $$\mathrm{IMF_j}(t) = \gamma_{j-1}(t) - \gamma_j(t).$$

7. Step 5 is repeated to obtain all the subsequent IMFs.

### 2.2. Extreme learning machine (ELM) model

ELM is an advanced data driven model introduced by Huang et al., [48] which utilizes a Single Layer Feed forward Neural Network (SLFN) to learn the pertinent predictive features from the historical data. ELM is comparatively faster and computationally convenient in relation to the existing data intelligent models [48–50]. The mathematical formulation of the ELM algorithm is as:

$$\sum_{i=1}^{M} \rho_i f(\mathrm{Hs_k}, c_i, w_i) = \mathrm{Hs_{For}} \tag{1}$$

In Eq. (1) $k$ ranges from 1 to M, which is the length of training data; the term $f(\mathrm{Hs_k}, c_i, w_i)$ denotes a nonlinear piecewise continuous activation function of features that take into account the assigned weights of the hidden neurons ($w_i \in \Gamma$) and the bias term ($c_i \in \Gamma$) corresponding to the respective input variable $\mathrm{Hs_k}$. $\mathrm{Hs_k}$ in this study is the antecedent lagged inputs of Hs sub-series. Further, $\rho_i$ represents the weight vector that connects the hidden node and the $i$th input nodes and $\mathrm{Hs_{For}}$ is the output or forecasted Hs as in this case.

Therefore, Eq. (1) reduces to the following form:

$$A\beta = Y \tag{2}$$

where $A = \begin{bmatrix} f(\mathrm{Hs_{k_1}}, c_1, w_1) & ... & f(\mathrm{Hs_{k_1}}, c_M, w_M) \\ \vdots & ... & \vdots \\ f(\mathrm{Hs_{k_N}}, c_1, w_1) & ... & f(\mathrm{Hs_{k_N}}, c_M, w_M) \end{bmatrix}_{N\times M}$, $\beta = (\beta_1^T\beta_2^T, ...,\beta_L^T)^T_{m\times M}$ and $Y = (\mathrm{Hs^T_{Obs_1}},\mathrm{Hs^T_{Obs_2}}, ...,\mathrm{Hs^T_{Obs_L}})^T_{m\times M}$. The output weight is obtained by the solution of the following linear system:

$$\beta = A^{-}Y \tag{3}$$

where $A^{-}$ is the Moore–Penrose generalized inverse of matrix A. The random input weight selection process adopted by the SLFNs are computationally efficient with lesser possibility of forecasting errors [51,52].

### 2.3. Online sequential extreme learning machine (OSELM) model

The traditional ELM uses each M-sample of data in the training period, but data may be used chunk-by-chunk in real-life problems. Consequently, the learning strategy may become time exhausting in traditional ELM whereby the training data set would be updated each time to run the model. As a variant of the traditional ELM model, the OSELM is developed in two learning steps *i.e.*, initialization and a sequential learning steps. In OSELM, the matrix A is packed in the initialization step and utilized in the next learning stage. During initialization, the weights and biases are assigned randomly to the small chunk of initial $\mathrm{H_S}$ training data to compute the hidden layer output matrix. The sequential learning phase then takes place either on a one-by-one or lump-by-lump basis avoiding the repetition of data usage. For more details on OSELM, the readers can refer to [53–55].

### 2.4. Random forest (RF) model

To ascertain a robust forecasting model, the skill of the proposed ICEEMDAN-ELM model is benchmarked with a random forest (RF) model. It is worthy to note that the ensemble learning strategies *e.g.*, bootstrapping and aggregation, initiates classifiers and aggregates them as decision trees [56,57]. The RF model adopts the technique of bagging with an extra randomness layer in the prediction procedure [57]. A randomly selected sample is assigned to each split node that enhances the performance and avoids overfitting [58]. Two parameters, *i.e.*, the number of trees in the forest and the number of terminal nodes/leaf, need to be predefined in RF models. The strategy of RF can be presented as:

*Step 1*

Build a bootstrapping of $n_{\mathrm{trees}}$ using the significant lag of IMFs at ($t$-1) of the $\mathrm{H_S}$ data where $n_{\mathrm{trees}}$ represents the number of trees in the forest ($n_{\mathrm{trees}}$ = 500 in this study).

*Step 2*

Then, trees of unprunned regressions with Hs are developed with the specified maximum number of terminal nodes/leaf represented as $m_{try}$ ($m_{try}$ = 5 generated optimal results in this study and have been adopted).

*Step 3*

Finally, the predictions of $n_{\mathrm{trees}}$ are aggregated to get the forecasted $\mathrm{Hs_{For}}$.

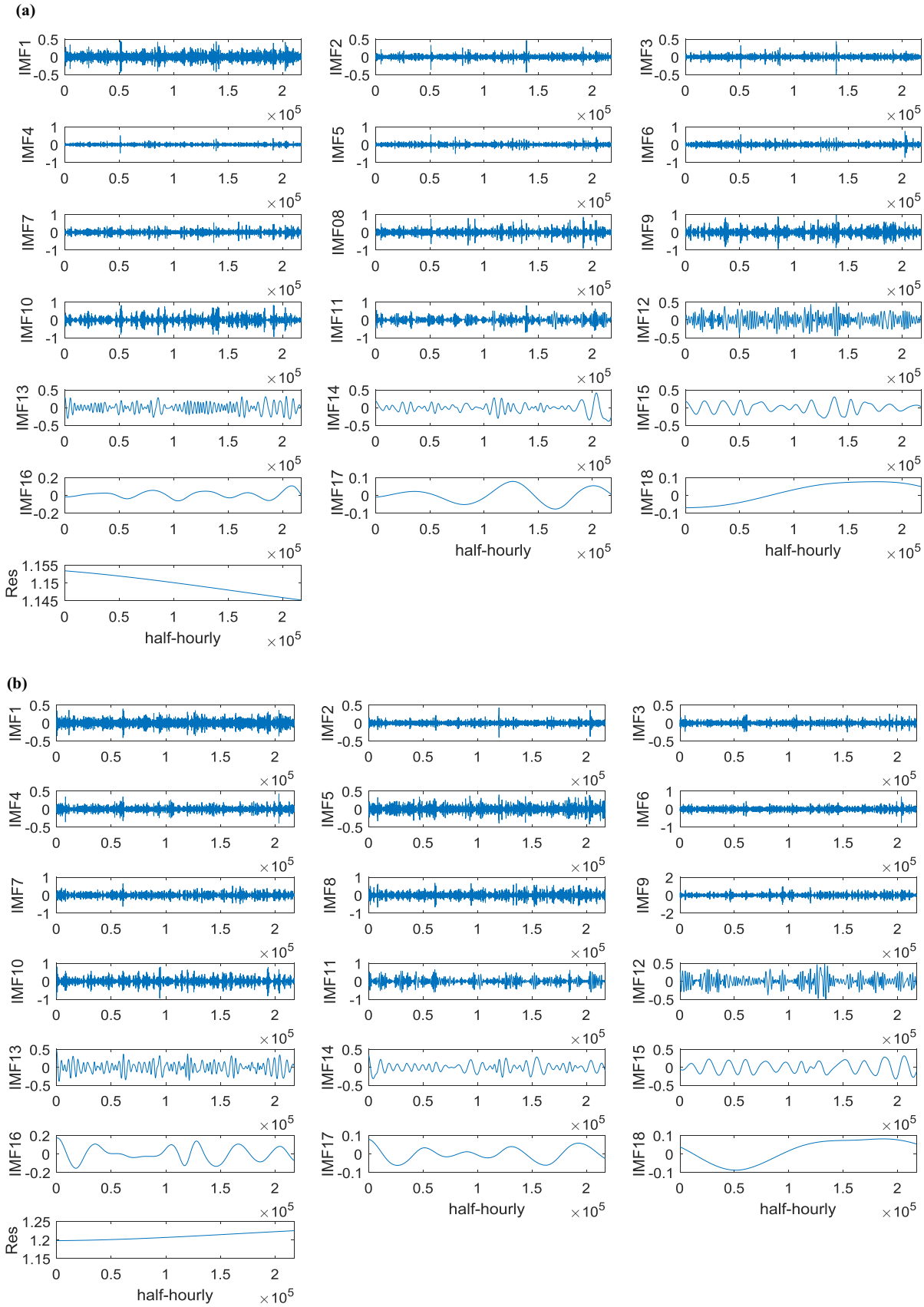


**Fig. 2.** Intrinsic mode functions (IMFs) and a residual component of significant wave height time series using ICEEMDAN for (a) Gold Coast station, and (b) Mooloolaba station during the training period. [NB: A total of 223944 data points were used during training, that is displayed as $2.2 \times 10^5$].

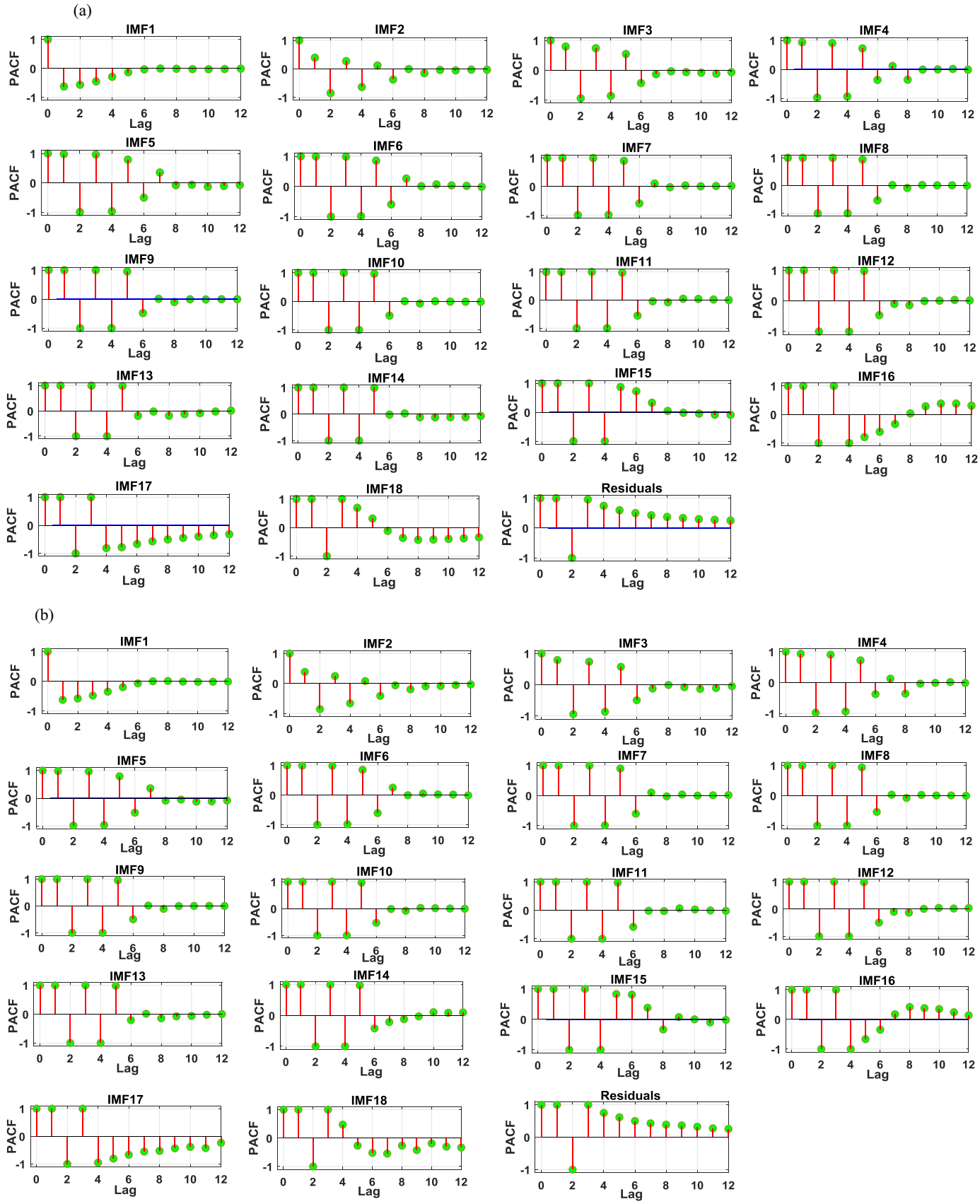


**Fig. 3.** Statistically significant *PACF* of IMFs and residual used for developing the ICEEMDAN-ELM model at (a) Gold Coast station, and (b) Mooloolaba station.

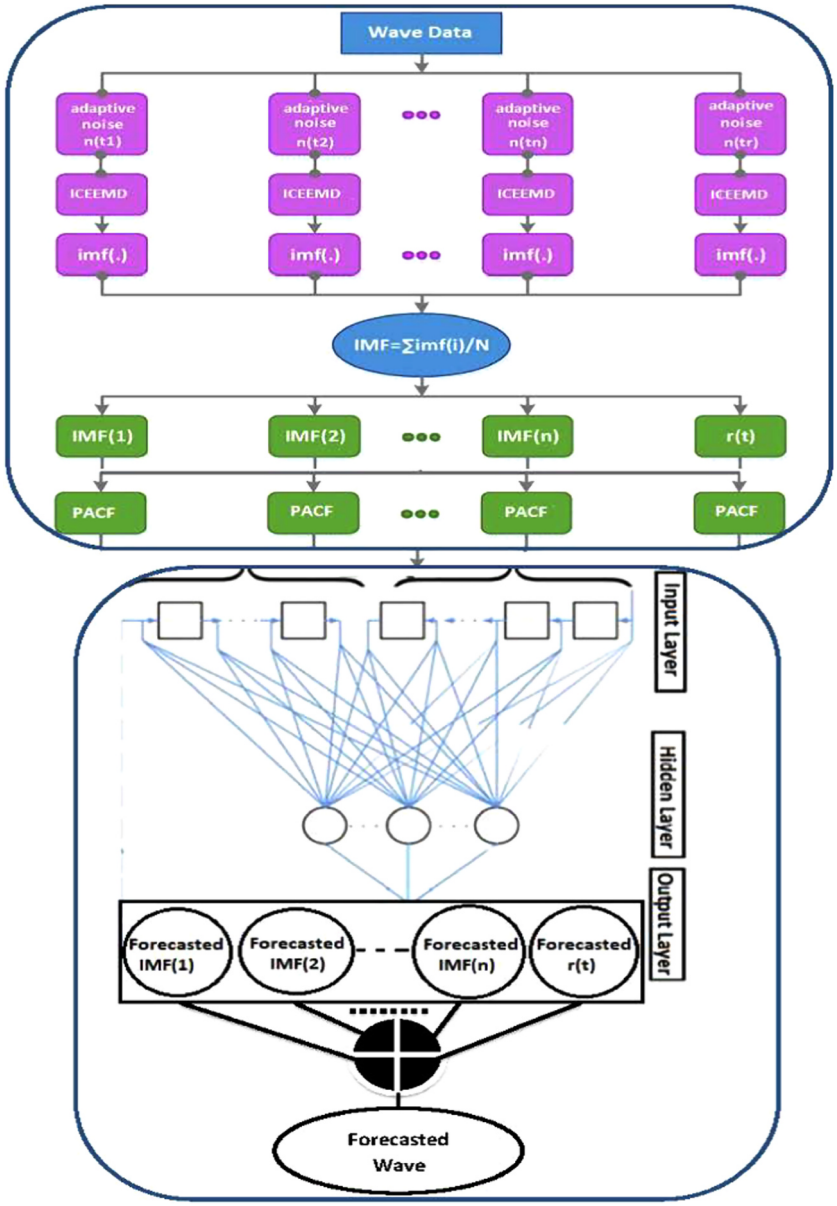


**Fig. 4.** Flowchart of the proposed hybrid two-phase ICEEMDAN-ELM model.

A detailed literature on the applications of RF can be found in [58–61].

## 3. Materials and methods

### 3.1. Study region and wave height dataset

In this paper, we have utilized the Hs data (in meters) obtained from the Environment and Science, Queensland Government, Coastal Data System, Queensland, Australia from January-2000 to March-2018 [62] for the two selected coastal regions, Gold Coast and Mooloolaba, as shown in Fig. 1. At respective sites, the Hs data is acquired at half-hourly intervals using Datawell Waverider wave-monitoring buoys.

To evaluate the versatility of the proposed ICEEMDAN-ELM model for Hs forecasting in Queensland's coastline, the study sites were chosen carefully to ensure that they were broadly representative of the diverse climatic conditions. The study sites Gold Coast and Mooloolaba are coastal cities located in the south-eastern region of the state of Queensland, Australia [63]. Table 1 demonstrates the basic statistics of Gold Coast and Mooloolaba stations. The annual mean integrated energy flux at coastlines adjacent to southern Queensland state (off the Gold Coast and Mooloolaba coastline) has been estimated to be 44 TWh/yr (at 25 m contour) and 53 TWh/yr (at 50 m contour) [64]. The close proximity of these cities to potential ocean wave energy resources would allow for the economical harnessing of energy using suitable wave energy converters.

### 3.2. Development of the ICEEMDAN-ELM model

The proposed ICEEMDAN-ELM model was developed using MATLAB R2017b, (The Math Works Inc. USA) with Pentium 4, 2.93 GHz dual-core central processing unit. Historical significant Hs time series data were used to develop the proposed ICEEMDAN-ELM model. The half-hourly Hs data utilized in this study was from January-2000 to March-2018 leading to a total of 319920 data points. All data were partitioned independently into training (70%), and testing (30%) sets to prevent the presence of future data into the input time series and the subsequent introduction of biases in the forecasts [65,66]. The development of the proposed ICEEMDAN-ELM model involved the following steps:

**Table 2**
The model development framework for a) standalone ELM, b) standalone OSELM model with *sin* transfer function and c) the standalone random forest at Gold Coast and Mooloolaba sites.

| Sites | a) Standalone ELM | | | a) Standalone OSELM | | | a) Standalone random forest | | | | | | | | | |
|---|---|---|---|---|---|---|---|---|---|---|---|---|---|---|---|---|
| | No. of neurons | | | | | | Delta criterion decision split ($C$) | | | | Number of predictor split ($N_p$) | | | | Permuted predictor delta error ($E_D$) | |
| | Input layer | Hidden layer | Output layer | Hidden layer | No. block | Output layer | | | | | | | | | | |
| Gold Coast | 3 | 2 | 1 | 9 | 10 | 1 | 0.044 | 0.048 | 0.045 | 0.040 | 818,268 | 1,020,218 | 1,263,983 | 1,424,243 | 2.044 | 1.089 | 0.673 | 1.995 |
| Mooloolaba | 3 | 7 | 1 | 8 | 10 | 1 | 0.034 | 0.035 | 0.031 | | 1,123,430 | 1,122,526 | 1,124,810 | | 1.609 | 1.113 | 1.062 | |

*Step 1*

The ICEEMDAN algorithm is used to decompose the Hs data into respective IMFs and a residual component for model development. Additionally, the predefined parameters used included the number of realizations of the Gaussian Noise or ensemble number ($N = 500$) and the amplitude of the added white noise ($\varepsilon = 0.2$) [36,67–69]. For Gold Coast and Mooloolaba sites, the ICEEMDAN algorithm decomposed the Hs data into eighteen (18) IMF sub-series (IMF1, IMF2,…, IMF18) and a residual component. Fig. 2 illustrates the ICEEMDAN decomposed Hs data series in IMFs with the residual for both the study sites.

*Step 2*

Next, using the partial autocorrelation function (PACF), statistically significant lag time series of respective IMFs and residual component were determined as shown in Fig. 3.

*Step 3*

The normalization of the significant lags of IMFs and residuals was accomplished following Eq. (4) to overcome data fluctuation caused by the features and patterns [70] as below:

$$\mathrm{Hs}_{\mathrm{norm}} = \frac{(\mathrm{Hs} - \mathrm{Hs}_{\mathrm{min}})}{(\mathrm{Hs}_{\mathrm{max}} - \mathrm{Hs}_{\mathrm{min}})} \tag{4}$$

where Hs indicates input/target IMF values, $\mathrm{Hs}_{\mathrm{min}}$ is the smallest value, $\mathrm{Hs}_{\mathrm{max}}$ is the largest value in the dataset and $\mathrm{Hs}_{\mathrm{norm}}$ is the desired normalized value.

*Step 4*

After incorporating the normalized antecedent significant lags of IMFs and residual as the input predictor in the ELM model, the respective IMFs, and the residual component were forecasted one at a time. Different activation functions (sigmoid, sine, hardlim and radial basis) were tested to determine the best activation function. The sine function (*sin*) was found optimal with different numbers of hidden neurons ranging from 1 to 10 in the development of ICEEMDAN-ELM model.

*Step 5*

Finally, the forecasted IMFs and the residual were aggregated to determine the forecasted Hs values. Fig. 4 shows the schematic view of the proposed ICEEMDAN-ELM model.

For a robust evaluation of ICEEMDAN-ELM model, OSELM and RF models were also integrated with ICEEMDAN. Further to that, the standalone ELM, OSELM and RF models were also tested in forecasting of Hs data. Table 2 illustrates the modeling framework of standalone ELM, OSELM, and RF models, and Table 3(a–b) shows the model development framework of the proposed ICEEMDAN-ELM *vs.* ICEEMDAN-OSELM. While Table 4a–b demonstrates the modeling framework during the development phase of ICEEMDAN-RF models at the respective sites.

### 3.3. Model performance evaluation criteria

To evaluate the performance of the proposed ICEEMDAN-ELM *vs.* ICEEMDAN-OSELM, ICEEMDAN-RF, and the standalone models (ELM, OSELM, and RF) applied for Hs forecasting, statistical and standardized metrics [71] were used. The mathematical formulations of these assessment metrics are given as follows [72–77].

I. Correlation coefficient ($r$) is expressed as:

$$r = \frac{\sum_{i=1}^{N} (\mathrm{Hs}_{\mathrm{Obs},i} - \overline{\mathrm{Hs}}_{\mathrm{Obs},i})(\mathrm{Hs}_{\mathrm{For},i} - \overline{\mathrm{Hs}}_{\mathrm{For},i})}{\sqrt{\sum_{i=1}^{N} (\mathrm{Hs}_{\mathrm{Obs},i} - \overline{\mathrm{Hs}}_{\mathrm{Obs},i})^2}\sqrt{\sum_{i=1}^{N} (\mathrm{Hs}_{\mathrm{For},i} - \overline{\mathrm{Hs}}_{\mathrm{For},i})^2}} \tag{5}$$

II. Willmott's Index ($WI$) is expressed as:

**Table 3**
The model development framework of ICEEMDAN-ELM *vs.* ICEEMDAN-OSELM at a) Gold Coast and b) Mooloolaba sites with *sin* transfer function.

| | a) **Gold Coast** | | | | | | a) **Mooloolaba** | | | | | |
|---|---|---|---|---|---|---|---|---|---|---|---|---|
| | **ICEEMDAN-ELM** | | | **ICEEMDAN-OSELM** | | | **ICEEMDAN-ELM** | | | **ICEEMDAN-OSELM** | | |
| | **No. of neurons** | | | **No. of neurons** | | | **No. of neurons** | | | **No. of neurons** | | |
| IMF Nos. | **Input layer** | **Hidden layer** | **Output layer** | **Input layer** | **Hidden layer** | **Output layer** | **Input layer** | **Hidden layer** | **Output layer** | **Input layer** | **Hidden layer** | **Output layer** |
| IMF1 | 5 | 8 | 1 | 5 | 7 | 1 | 6 | 9 | 1 | 6 | 7 | 1 |
| IMF2 | | 8 | | | 8 | | | 7 | | | 10 | |
| IMF3 | | 10 | | | 9 | | | 10 | | | 6 | |
| IMF4 | | 9 | | | 9 | | | 10 | | | 6 | |
| IMF5 | | 10 | | | 7 | | | 10 | | | 8 | |
| IMF6 | | 10 | | | 5 | | | 10 | | | 8 | |
| IMF7 | | 10 | | | 5 | | | 10 | | | 3 | |
| IMF8 | | 10 | | | 7 | | | 10 | | | 5 | |
| IMF9 | | 10 | | | 5 | | | 10 | | | 2 | |
| IMF10 | | 10 | | | 9 | | | 10 | | | 5 | |
| IMF11 | | 10 | | | 5 | | | 10 | | | 5 | |
| IMF12 | | 10 | | | 7 | | | 10 | | | 2 | |
| IMF13 | | 10 | | | 10 | | | 10 | | | 2 | |
| IMF14 | | 10 | | | 7 | | | 10 | | | 2 | |
| IMF15 | | 10 | | | 7 | | | 10 | | | 5 | |
| IMF16 | | 9 | | | 5 | | | 10 | | | 10 | |
| IMF17 | | 9 | | | 9 | | | 10 | | | 7 | |
| IMF18 | | 10 | | | 5 | | | 10 | | | 10 | |
| Residual | | 10 | | | 5 | | | 9 | | | 6 | |

$$WI = 1 - \left[ \frac{\sum_{i=1}^{N} (\mathrm{Hs}_{\mathrm{For},i} - \mathrm{Hs}_{\mathrm{Obs},i})^2}{\sum_{i=1}^{N} (|\mathrm{Hs}_{\mathrm{For},i} - \bar{\mathrm{H}}s_{\mathrm{Obs},\ i}| + |\mathrm{Hs}_{\mathrm{Obs},i} - \bar{\mathrm{H}}s_{\mathrm{Obs},i}|)^2} \right], \quad 0 \le WI \le 1 \tag{6}$$

III. Nash-Sutcliffe coefficient ($E_{NS}$) is expressed as:

$$E_{NS} = 1 - \left[ \frac{\sum_{i=1}^{N} (\mathrm{Hs}_{\mathrm{Obs},i} - \mathrm{Hs}_{\mathrm{For},i})^2}{\sum_{i=1}^{N} (\mathrm{H}_{\mathrm{Obs},i} - \overline{\mathrm{Hs}}_{\mathrm{For},i})^2} \right], \quad 0 \le E_{NS} \le 1 \tag{7}$$

IV. Root mean square error (*RMSE, m*) is expressed as:

$$RMSE = \sqrt{\frac{1}{N} \sum_{i=1}^{N} (\mathrm{Hs}_{\mathrm{For},\ i} - H_{\mathrm{Obs},\ i})^2} \tag{8}$$

V. Mean absolute error (*MAE, m*) is expressed as:

$$MAE = \frac{1}{N} \sum_{i=1}^{N} |\mathrm{Hs}_{\mathrm{For},i} - H_{\mathrm{Obs},i}| \tag{9}$$

VI. Legates-McCabe's (*LM*) is expressed as:

$$LM = 1 - \left[ \frac{\sum_{i=1}^{N} |\mathrm{Hs}_{\mathrm{For},i} - \mathrm{Hs}_{\mathrm{Obs},i}|}{\sum_{i=1}^{N} |\mathrm{Hs}_{\mathrm{Obs},i} - \bar{\mathrm{H}}s_{\mathrm{Obs},i}|} \right], \quad 0 \le LM \le 1 \tag{10}$$

VII. Relative root mean square error (*RRMSE*,%) is expressed as:

$$RRMSE = \frac{\sqrt{\frac{1}{N} \sum_{i=1}^{N} (\mathrm{H}_{\mathrm{For},\ i} - \mathrm{Hs}_{\mathrm{Obs},\ i})^2}}{\frac{1}{N} \sum_{i=1}^{N} (\mathrm{Hs}_{\mathrm{Obs},\ i})} \times 100 \tag{11}$$

VIII. Relative mean absolute percentage error (*RMAE*; %), is expressed as

$$RMAE = \frac{1}{N} \sum_{i=1}^{N} \left| \frac{\mathrm{Hs}_{\mathrm{For},\ i} - \mathrm{Hs}_{\mathrm{Obs},\ i}}{\mathrm{Hs}_{\mathrm{Obs},\ i}} \right| \times 100 \tag{12}$$

where $\mathrm{Hs}_{\mathrm{Obs},i}$ and $\mathrm{Hs}_{\mathrm{For},\ i}$ are the observed and forecasted ith value of the significant wave height Hs, $\overline{\mathrm{Hs}}_{\mathrm{Obs},i}$ and $\overline{\mathrm{Hs}}_{\mathrm{For},i}$ are the average values of observed and forecasted Hs and $N$ is the total number of tested data points.

## 4. Results

The proposed ICEEMDAN-ELM is appraised in comparison with ICEEMDAN-OSELM, ICEEMDAN-RF, standalone ELM, standalone OSELM, and standalone RF models, using statistical metrics, diagnostic plots and error distributions (Eqs. (5)–(12)) between the forecasted and observed Hs.

In Table 5, the preciseness of the ICEEMDAN-ELM is evaluated in relation to the respective models *i.e.*, ICEEMDAN-OSELM, ICEEMDAN-RF, standalone ELM, OSELM and RF models where the results for each tested site are shown on the basis of *r*, *RMSE,* and *MAE*. The ICEEMDAN-ELM model applied at Gold Coast site attained the highest correlation coefficient and smallest *RMSE* and *MAE* as compared to the ICEEMDAN-OSELM, ICEEMDAN-RF, standalone ELM, OSELM and RF model (Table 5). Similarly, the performance of the ICEEMDAN-ELM model is better for Mooloolaba site followed by ICEEMDAN-RF, ICEEMDAN-OSELM, standalone RF, ELM and OSELM models in terms of achieving the largest magnitudes of *r* and smallest magnitudes of *RMSE* and *MAE*. This is a clear indication that the proposed ICEEMDAN-ELM model can be considered to be a better data-intelligent tool for Hs forecasting as compared to the other models.

Further analysis *via* the empirical cumulative distribution function (ECDF, Fig. 5) at each station was carried out to depict the different forecasting skills in terms of absolute forecasting error, |FE|. FE is the difference between the forecasted and observed Hs, *i.e.*, $\mathrm{FE} = \mathrm{Hs}_{\mathrm{For},i} - \mathrm{Hs}_{\mathrm{Obs},i}$ which ideally must be 0. As a result, for a better forecasting model higher frequencies of the forecasting error value ought to be closer to zero. In comparison to the standalone ELM, standalone OSELM and standalone RF models, the hybrid ICEEMDAN-ELM, ICEEMDAN-OSELM and ICEEMDAN-RF are the more accurate models, with slightly higher accuracy portrayed by the ICEEMDAN-ELM. Based on the error (0 to ± 2.0 m) for the Gold Coast and Mooloolaba stations, Fig. 5 clearly shows that the ICEEMDAN-ELM method was the most accurate model in forecasting Hs.

**Table 4**
The model development framework for the random forest models *i.e.*, ICEEMDAN-RF at a) Gold Coast and b) Mooloolaba sites.

a) **Gold Coast**

| | Delta criterion decision split ($C$) | | | | | Number of predictor split ($N_p$) | | | | | Permuted predictor delta error ($E_D$) | | | | |
|---|---|---|---|---|---|---|---|---|---|---|---|---|---|---|---|
| **IMF1** | 0.003 | 0.001 | 0.001 | 0.001 | 0.000 | 2,159,072 | 2,198,090 | 2,239,561 | 2,261,734 | 2,214,774 | 37.640 | 12.158 | 5.765 | 3.748 | 2.497 |
| **IMF2** | 0.000 | 0.001 | 0.001 | 0.000 | 0.000 | 2,082,737 | 2,079,411 | 2,075,302 | 2,102,263 | 2,056,037 | 6.336 | 8.649 | 2.420 | 4.719 | 3.516 |
| **IMF3** | 0.001 | 0.000 | 0.000 | 0.001 | 0.001 | 1,217,189 | 1,245,250 | 1,189,014 | 1,174,796 | 1,184,903 | 7.361 | 4.533 | 2.876 | 2.507 | 1.493 |
| **IMF4** | 0.008 | 0.004 | 0.002 | 0.001 | 0.002 | 623,786 | 610,268 | 591,684 | 579,528 | 561,832 | 4.356 | 1.588 | 1.701 | 1.322 | 1.353 |
| **IMF5** | 0.033 | 0.025 | 0.018 | 0.012 | 0.009 | 303,478 | 291,527 | 287,535 | 280,481 | 269,980 | 2.663 | 1.226 | 0.844 | 0.787 | 1.828 |
| **IMF6** | 0.066 | 0.053 | 0.050 | 0.046 | 0.035 | 156,517 | 155,203 | 150,845 | 149,814 | 150,214 | 2.125 | 1.225 | 0.888 | 0.806 | 2.117 |
| **IMF7** | 0.290 | 0.264 | 0.255 | 0.256 | 0.244 | 100,716 | 99,237 | 97,740 | 96,139 | 97,295 | 1.873 | 1.191 | 0.803 | 0.690 | 3.260 |
| **IMF8** | 0.494 | 0.526 | 0.449 | 0.514 | 0.498 | 69,499 | 68,132 | 67,028 | 65,861 | 66,028 | 1.527 | 1.180 | 0.826 | 0.577 | 3.589 |
| **IMF9** | 1.362 | 1.415 | 1.279 | 1.447 | 1.346 | 47,333 | 46,237 | 44,986 | 43,635 | 42,981 | 1.407 | 1.108 | 0.737 | 0.544 | 5.297 |
| **IMF10** | 2.757 | 2.792 | 3.032 | 3.349 | 2.958 | 32,403 | 32,268 | 31,525 | 30,185 | 29,200 | 1.268 | 1.000 | 0.845 | 0.565 | 4.254 |
| **IMF11** | 4.493 | 4.940 | 4.022 | 4.211 | 4.478 | 22,789 | 22,865 | 22,793 | 22,610 | 21,711 | 1.259 | 1.039 | 0.759 | 0.464 | 0.250 |
| **IMF12** | 10.700 | 9.335 | 10.642 | 11.743 | 10.738 | 17,922 | 18,177 | 17,960 | 18,024 | 18,034 | 1.132 | 0.891 | 0.713 | 0.505 | 0.084 |
| **IMF13** | 21.543 | 20.881 | 21.541 | 20.044 | 22.073 | 13,301 | 13,874 | 13,621 | 13,602 | 13,722 | 1.177 | 0.949 | 0.726 | 0.459 | 0.138 |
| **IMF14** | 13.382 | 13.800 | 13.498 | 13.638 | 12.331 | 15,245 | 15,177 | 15,071 | 15,296 | 14,963 | 1.363 | 1.079 | 0.719 | 0.496 | 0.094 |
| **IMF15** | 31.015 | 27.773 | 28.982 | 25.876 | 29.666 | 11,888 | 11,866 | 11,896 | 12,095 | 11,913 | 1.155 | 0.888 | 0.664 | 0.455 | 0.086 |
| **IMF16** | 9.887 | 10.152 | 8.826 | 10.031 | 9.891 | 12,929 | 13,022 | 13,085 | 13,098 | 13,044 | 1.156 | 0.948 | 0.705 | 0.453 | 0.073 |
| **IMF17** | 47.031 | 43.497 | 41.538 | 41.919 | 39.487 | 11,291 | 11,265 | 11,282 | 11,056 | 11,262 | 1.224 | 0.890 | 0.651 | 0.419 | 0.130 |
| **IMF18** | 105.624 | 92.470 | 97.908 | 97.464 | 88.169 | 9888 | 9757 | 9846 | 9911 | 9798 | 0.600 | 0.592 | 0.621 | 0.591 | 0.527 |
| **Residual** | 40.777 | 42.382 | 33.913 | 37.818 | 39.749 | 10,180 | 10,272 | 10,028 | 10,175 | 10,145 | 0.632 | 0.716 | 0.611 | 0.584 | 0.689 |

a) **Mooloolaba**

| | Delta criterion decision split ($C$) | | | | | | Number of predictor split ($N_p$) | | | | | | Permuted predictor delta error ($E_D$) | | | | | |
|---|---|---|---|---|---|---|---|---|---|---|---|---|---|---|---|---|---|---|
| **IMF1** | 0.006 | 0.002 | 0.001 | 0.001 | 0.001 | 0.001 | 1,743,620 | 1,775,811 | 1,792,832 | 1,792,782 | 1,782,032 | 1,757,706 | 23.355 | 9.411 | 5.146 | 2.940 | 2.714 | 2.429 |
| **IMF2** | 0.001 | 0.001 | 0.001 | 0.000 | 0.000 | 0.000 | 1,677,348 | 1,687,075 | 1,657,626 | 1,711,569 | 1,652,700 | 1,677,046 | 4.868 | 7.388 | 2.234 | 4.027 | 3.078 | 2.441 |
| **IMF3** | 0.005 | 0.002 | 0.002 | 0.003 | 0.002 | 0.001 | 1,082,027 | 1,088,014 | 1,035,702 | 1,022,174 | 1,033,470 | 1,039,706 | 5.216 | 3.787 | 3.155 | 2.225 | 1.573 | 2.264 |
| **IMF4** | 0.010 | 0.005 | 0.003 | 0.002 | 0.002 | 0.003 | 601,167 | 574,833 | 566,173 | 549,591 | 542,253 | 519,377 | 4.130 | 1.726 | 1.908 | 2.041 | 1.069 | 1.248 |
| **IMF5** | 0.030 | 0.024 | 0.017 | 0.011 | 0.008 | 0.005 | 283,882 | 267,268 | 265,096 | 261,610 | 255,525 | 250,927 | 2.323 | 1.376 | 0.865 | 0.952 | 0.937 | 1.882 |
| **IMF6** | 0.059 | 0.051 | 0.047 | 0.034 | 0.028 | 0.024 | 148,458 | 145,055 | 140,895 | 138,674 | 137,753 | 136,076 | 1.709 | 1.217 | 0.895 | 0.685 | 0.810 | 1.851 |
| **IMF7** | 0.211 | 0.204 | 0.206 | 0.179 | 0.166 | 0.173 | 89,007 | 87,448 | 85,886 | 84,069 | 84,346 | 85,480 | 1.466 | 1.136 | 1.006 | 0.668 | 0.496 | 2.144 |
| **IMF8** | 0.605 | 0.642 | 0.545 | 0.537 | 0.521 | 0.548 | 60,509 | 59,320 | 58,123 | 56,768 | 56,519 | 56,890 | 1.321 | 1.138 | 0.823 | 0.565 | 0.416 | 3.273 |
| **IMF9** | 1.000 | 1.094 | 0.993 | 1.095 | 0.970 | 1.009 | 41,661 | 41,521 | 40,536 | 39,081 | 38,224 | 38,160 | 1.221 | 0.997 | 0.813 | 0.595 | 0.374 | 4.124 |
| **IMF10** | 2.107 | 1.833 | 2.070 | 1.970 | 1.992 | 1.954 | 29,657 | 29,319 | 28,917 | 28,165 | 26,915 | 26,373 | 1.160 | 0.904 | 0.740 | 0.621 | 0.402 | 3.850 |
| **IMF11** | 5.009 | 5.017 | 5.126 | 4.944 | 4.854 | 4.983 | 20,358 | 20,058 | 20,132 | 20,089 | 19,574 | 18,913 | 1.119 | 0.961 | 0.735 | 0.557 | 0.380 | 2.803 |
| **IMF12** | 6.939 | 6.438 | 6.034 | 5.912 | 7.040 | 6.009 | 16,320 | 16,444 | 16,039 | 16,189 | 16,204 | 16,136 | 1.105 | 0.865 | 0.743 | 0.550 | 0.379 | 0.140 |
| **IMF13** | 9.095 | 10.056 | 9.832 | 9.623 | 10.450 | 10.153 | 13,310 | 13,337 | 13,295 | 13,191 | 13,027 | 13,164 | 0.939 | 0.895 | 0.739 | 0.537 | 0.407 | 0.259 |
| **IMF14** | 10.806 | 11.857 | 10.471 | 11.284 | 13.636 | 11.993 | 11,881 | 12,074 | 11,918 | 11,866 | 11,916 | 12,093 | 0.969 | 0.894 | 0.658 | 0.549 | 0.467 | 0.348 |
| **IMF15** | 24.969 | 27.725 | 28.870 | 26.941 | 24.551 | 22.308 | 9873 | 9809 | 9787 | 9909 | 9900 | 9808 | 0.877 | 0.836 | 0.694 | 0.473 | 0.329 | 0.122 |
| **IMF16** | 26.060 | 23.492 | 25.969 | 22.018 | 24.149 | 27.505 | 10,246 | 10,160 | 10,060 | 9980 | 10,274 | 10,170 | 0.997 | 0.761 | 0.746 | 0.513 | 0.394 | 0.328 |
| **IMF17** | 28.607 | 31.731 | 30.123 | 30.979 | 29.903 | 26.002 | 9489 | 9593 | 9561 | 9522 | 9536 | 9665 | 0.932 | 0.899 | 0.676 | 0.565 | 0.337 | 0.322 |
| **IMF18** | 55.016 | 81.742 | 80.056 | 58.645 | 85.002 | 76.843 | 8446 | 8437 | 8470 | 8622 | 8436 | 8389 | 0.682 | 0.778 | 0.627 | 0.473 | 0.436 | 0.483 |
| **Res.** | 29.999 | 31.002 | 28.206 | 33.629 | 29.819 | 29.931 | 8395 | 8571 | 8406 | 8501 | 8455 | 8472 | 0.566 | 0.526 | 0.518 | 0.625 | 0.534 | 0.564 |

**Table 5**
The performance evaluation of hybrid ICEEMDAN-ELM in comparison to ICEEMDAN-OS-ELM, ICEEMDAN-RF and the standalone ELM, standalone OSELM and standalone RF models applied in forecasting of significant wave height in the testing period based on Pearson's correlation coefficient (*r*); root mean square error (*RMSE*) and mean absolute error (*MAE*). The optimal models yielding the lowest *RMSE* at each site are shown in **boldface**.

| Model | Performance metrics | Sites | |
|---|---|---|---|
| | | Gold Coast | Mooloolaba |
| **Random forest** | *r* | 0.989 | 0.990 |
| | *RMSE* (m) | 0.068 | 0.070 |
| | *MAE* (m) | 0.048 | 0.050 |
| **Online sequential ELM (OSELM)** | *r* | 0.982 | 0.962 |
| | *RMSE* (m) | 0.085 | 0.136 |
| | *MAE* (m) | 0.059 | 0.093 |
| **Extreme learning machine (ELM)** | *r* | 0.992 | 0.962 |
| | *RMSE* (m) | 0.056 | 0.136 |
| | *MAE* (m) | 0.039 | 0.093 |
| **ICEEMDAN-RF** | *r* | 0.998 | **0.999** |
| | *RMSE* (m) | 0.034 | 0.020 |
| | *MAE* (m) | 0.025 | 0.013 |
| **ICEEMDAN-OSELM** | *r* | **0.999** | **0.999** |
| | *RMSE* (m) | 0.017 | 0.023 |
| | *MAE* (m) | 0.011 | 0.016 |
| **ICEEMDAN-ELM** | *r* | **0.999** | **0.999** |
| | *RMSE* (m) | **0.016** | **0.018** |
| | *MAE* (m) | **0.010** | **0.012** |

To further ascertain the better performance of hybrid ICEEMDAN-ELM model, Fig. 6 compares boxplots of the ICEEMDAN-ELM model with ICEEMDAN-OSELM, ICEEMDAN-RF, standalone ELM, OSELM and RF models for each station. The + denotes the outliers of the extreme absolute forecasting error, |FE|, of the testing data together with their upper quartile, median, and lower quartile. The smaller distribution of |FE| with a much smaller quartile range was acquired by the ICEEMDAN-ELM model for Gold Coast site, followed by the ICEEMDAN-OSELM, ICEEMDAN-RF and the standalone ELM, OSELM and RF models. Similarly, the ICEEMDAN-ELM model again achieved a good accuracy in terms of |FE| distributions for Mooloolaba stations in relation to the counterpart models. By means of Fig. 6, the accuracy of the ICEEMDAN-ELM model for both stations appeared to be better than the other competing models, *i.e.*, ICEEMDAN-OSELM, ICEEMDAN-RF and standalone ELM, OSELM and RF models. This further confirms the suitability of the ICEEMDAN-ELM in forecasting half-hourly Hs values.

In addition, Table 6 presents the accuracy of the hybrid ICEEMDAN-ELM model in comparison to other models developed in this study, evaluated for both stations in terms of *WI*, $E_{NS}$, and *LM*. The ICEEMDAN-ELM model in Gold Coast station attained the higher values of $WI \approx 0.999$, $E_{NS} \approx 0.999$ and $LM \approx 0.969$, and were followed by ICEEMDAN-OSELM ($WI \approx 0.999$, $E_{NS} \approx 0.999$, and $LM \approx 0.968$), ICEEMDAN-RF ($WI \approx 0.998$, $E_{NS} \approx 0.994$, and $LM \approx 0.927$), standalone ELM ($WI \approx 0.988$, $E_{NS} \approx 0.985$ and $LM \approx 0.883$), standalone RF ($WI \approx 0.991$, $E_{NS} \approx 0.977$ and $LM \approx 0.858$) and standalone OSELM ($WI \approx 0.974$, $E_{NS} \approx 0.965$ and $LM \approx 0.826$) models. For the other site Mooloolaba, the ICEEMDAN-RF, ICEEMDAN-ELM, and ICEEMDAN-OSELM have very close performances, yet the ICEEMDAN-ELM model appeared to have slightly better performance (see; Table 6) in comparison to the counterpart models. Thus, the ICEEMDAN-ELM model shows slightly higher predictive accuracy as compared to the other models in this study.

The goodness-of-fit and correlation coefficient *r* between predicted and observed Hs is displayed in the scatterplots (Fig. 7). The ICEEMDAN-ELM model is relatively better than ICEEMDAN-OSELM, ICEEMDAN-RF, standalone ELM, OSELM, and RF models in terms of $r^2$ (ICEEMDAN-ELM ≈ 0.9987, ICEEMDAN-OSELM ≈ 0.9986, ICEEMDAN-RF ≈ 0.9955, ELM ≈ 0.9847, OSELM ≈ 0.9651, RF ≈ 0.9774) for Gold Coast. Again, the hybrid ICEEMDAN-ELM model is more accurate for Mooloolaba, with the following $r^2$ values (ICEEMDAN-ELM ≈ 0.9987, ICEEMDAN-OSELM ≈ 0.9981, ICEEMDAN-RF ≈ 0.9985, ELM ≈ 0.9250, OSELM ≈ 0.9248, and RF ≈ 0.9799). On the basis of attaining the larger $r^2$-value, the ICEEMDAN-ELM model shows marginally better accuracy against the comparison models for both the study regions, further ascertaining the suitability of the proposed model.

The sites Gold Coast and Mooloolaba sites are at different locations with differing oceanic features and physiography. As such relative errors *i.e.*, relative root mean squared error (*RRMSE*) and relative mean absolute error (*RMAE*) are required for model comparison at these sites. Table 7 demonstrates the magnitudes of *RRMSE* and *RMAE*. Based on

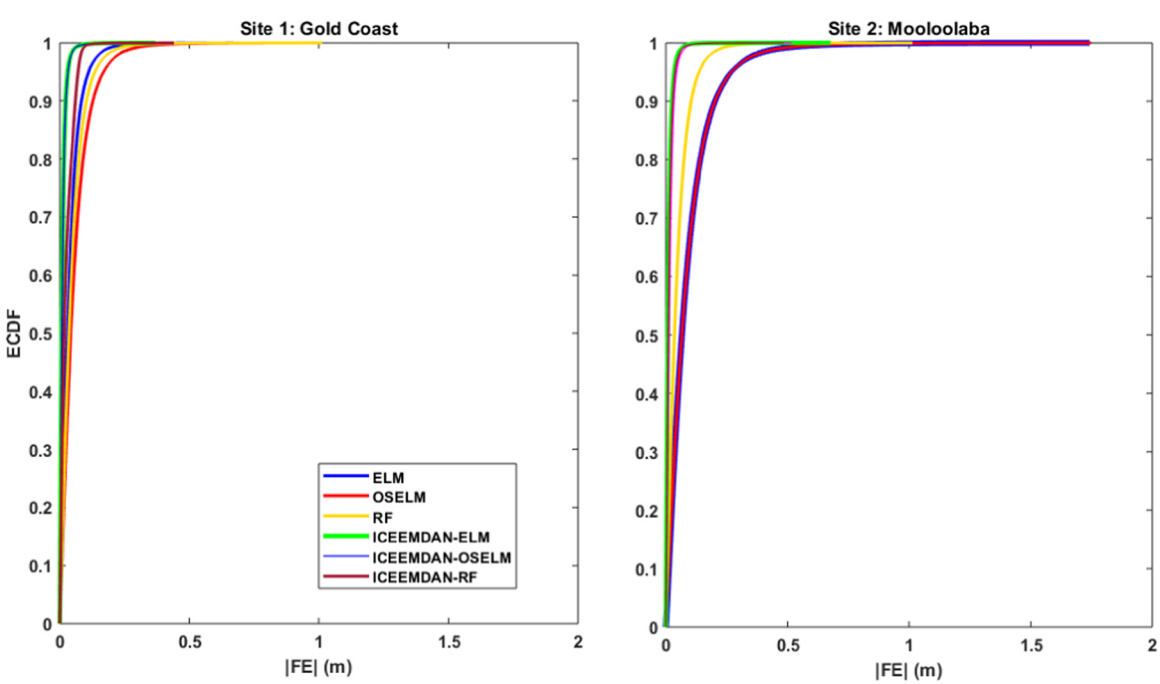


**Fig. 5.** Empirical cumulative distribution function (ECDF) of the absolute forecasting error, |FE| (m), of the testing stations using **ICEEMDAN-ELM** *vs.* ICEEMDAN-OSELM, ICEEMDAN-RF, ELM, OSELM, and RF models.

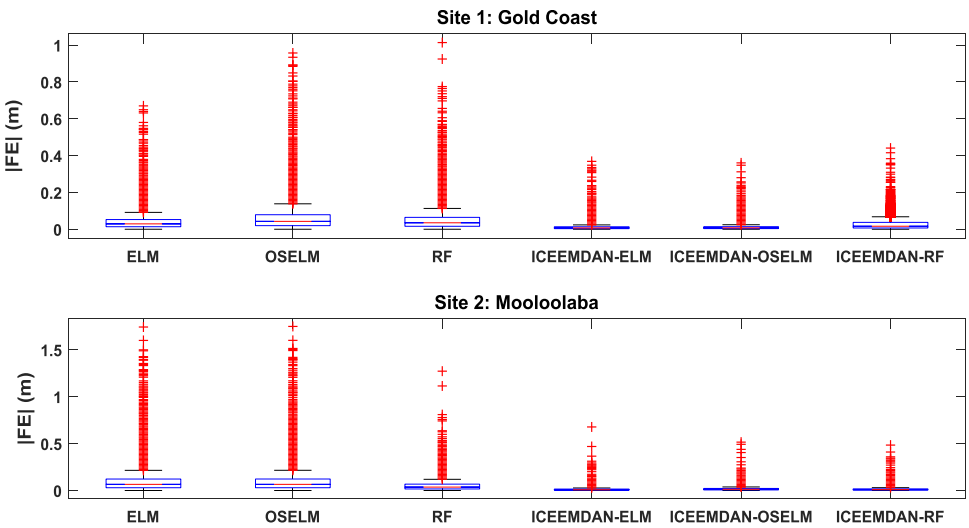


**Fig. 6.** Box-plots of absolute forecasted error, |FE| (m), of ICEEMDAN-ELM *vs.* ICEEMDAN-OSELM and ICEEMDAN-RF, ELM, OSELM and RF models between forecasted and observed significant wave height for Site 1: Gold Coast, and Site 2: Mooloolaba.

**Table 6**
The performance evaluation of ICEEMDAN-ELM in comparison to ICEEMDAN-OSELM, ICEEMDAN-RF and the standalone ELM, OSELM and RF models in forecasting significant wave height in the testing period based on Willmott's Index (*WI*); Nash–Sutcliffe Efficiency ($E_{NS}$) and Legates-McCabe's index (*LM*). The models with the largest value of the Legates-McCabe's index at each site are indicated in **boldface.**

| Model | Performance metrics | Sites | |
|---|---|---|---|
| | | Gold Coast | Mooloolaba |
| **Random forest** | *WI* | 0.991 | 0.992 |
| | $E_{NS}$ | 0.977 | 0.980 |
| | *LM* | 0.858 | 0.870 |
| **Online sequential ELM (OSELM)** | *WI* | 0.974 | 0.947 |
| | $E_{NS}$ | 0.965 | 0.924 |
| | *LM* | 0.826 | 0.759 |
| **Extreme learning machine (ELM)** | *WI* | 0.988 | 0.947 |
| | $E_{NS}$ | 0.985 | 0.924 |
| | *LM* | 0.883 | 0.759 |
| **ICEEMDAN-RF** | *WI* | 0.998 | **0.999** |
| | $E_{NS}$ | 0.994 | 0.998 |
| | *LM* | 0.927 | 0.965 |
| **ICEEMDAN-OSELM** | *WI* | **0.999** | **0.999** |
| | $E_{NS}$ | **0.999** | 0.998 |
| | *LM* | 0.968 | 0.957 |
| **ICEEMDAN-ELM** | *WI* | **0.999** | **0.999** |
| | $E_{NS}$ | **0.999** | **0.999** |
| | *LM* | **0.969** | **0.970** |

these relative measures, the proposed ICEEMDAN-ELM model was seen to generate the least relative percentage errors (*RRMSE, RMAE*) for both sites. Further to that, the ICEEMDAN-ELM model appeared to be most accurate one at Gold Coast site in forecasting Hs using with (*RRMSE* ≈ 1.51%) and (*RMAE* ≈ 0.93%). In addition to the forecasting errors generated by the proposed ICEEMDAN-ELM model were low in terms of their relative error values, but more importantly, they were within the recommended range of 10% threshold for an excellent model classification [78].

## 5. Discussions: merits, limitation, and further scope

The empirical mode decomposition is the lesser-explored data decomposition techniques used in Hs forecasting studies. In this pilot study, an advanced version of EMD *i.e.*, the ICEEMDAN [38] is explored. The half-hourly Hs data series were aptly decomposed *via* ICEEMDAN into respective IMFs and a residual component revealing the embedded features. The ICEEMDAN has proven to be a vital multi-resolution data pre-processing tool.

Integration of ICEEMDAN with the fast and efficient ELM [48] model, led to the newly developed ICEEMDAN-ELM model which effectively 'learns' these decomposed predictive features in emulating half-hourly Hs values. The better forecasting capability of ICEEMDAN-ELM in very near real-time (half -hourly) forecasting horizon is clear from the predictor metrics (Tables 5–7) and the diagnostic plots (Figs. 5–7) at both the study sites. The ELM algorithm is a fast and efficient SLFN. Together with ICEEMDAN which requires trivial human intervention, could possibly be used in near real-time forecasting of Hs. The key feature is that the performance of the newly developed hybrid ICEEMDAN-ELM model is relatively better with *WI* and $E_{NS}$ of 0.999 and *LM* ≥ 0.969 showing scaled precision of ICEEMDAN-ELM model in emulating half-hourly Hs values. Despite the studies being conducted at two geographically diverse sites with distinctive oceanographic features, the relative errors were also low in the range of *RRMSE* ≤ 1.51% and *RMAE* ≤ 0.96% affirming the universality of the ICEEMDAN-ELM model.

The wave energy is a potential natural resource for continental Australia [64] that can be feasibly harnessed from the surrounding ocean. Yet, the variability in the ocean wave is a vital factor that has been repressing the advancements in the ocean wave energy sector. Generally, the wave energy farms are capital-intensive requiring investor confidence and reliability [79]. As a result, amicable forecasting tools such as the newly proposed ICEEMDAN-ELM could provide enhanced forecasts allowing the energy engineers and decision makers to steadfastly harness the renewable ocean wave energy and generation of blue electricity. Additionally, the precise future estimates of wave energy parameter, Hs, using ICEEMDAN-ELM would also reinforce prudent planning and design optimization of reliable ocean energy converters [1,80].

Yet, the main challenges in very short-term forecasting applications are computational time and memory because efficiency and scalability become paramount in such near real-time purposes [81]. Fundamentally, the non-stationary Hs signal eventuates from nonlinear systems driving the Hs. Consequently, the ICEEMDAN demarcating method used in this study is beneficial for such applications due to its self-adaptive nature that entails minor manual tuning making it a suitable MRA tool for very short-time forecasting and real-time applications [82]. The ICEEMDAN has also shown to achieve a better result in comparison to the other EMD variants with even smaller ensemble sizes making ICEEMDAN computationally efficient [38]. In addition, there is a reduction in the amount of noise contained in the IMFs derived from ICEEMDAN decomposition. This would have enabled the ELM model to effectively extract features during modeling of Hs. Moreover, another important feature of ICEEMDAN is the avoidance of the spurious modes [38], which besides granting more physical meaning, significantly

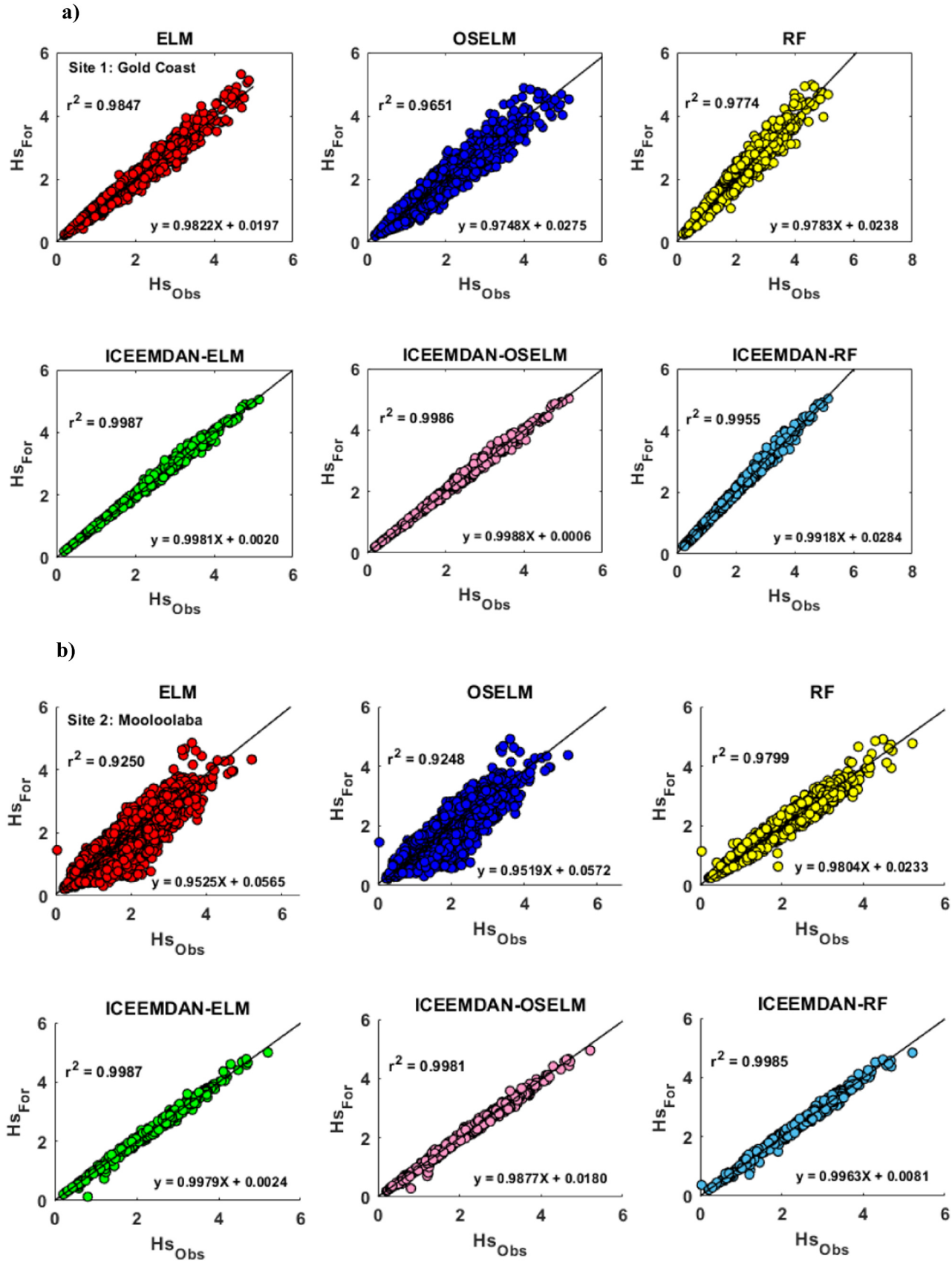


**Fig. 7.** Scatter-plots of forecasted and observed Hs using **ICEEMDAN-ELM** *vs.* ICEEMDAN-OSELM and ICEEMDAN-RF, ELM, OSELM, and RF models height for a) Site 1: Gold Coast, and b) Site 2: Mooloolaba. Also displayed are the coefficient of determination ($r^2$) and the equation of the linear fitting line.

**Table 7**
A comparison of performances of the ICEEMDAN-ELM and the comparative models at different sites using the relative error measures, relative root mean square error (*RRMSE*) and relative mean absolute error (*RMAE*) in forecasting of significant wave height. The optimal model with lowest relative (%) error is shown in **boldface.**

| Model | Relative performances (%) | Sites | |
|---|---|---|---|
| | | Gold Coast | Mooloolaba |
| **RF** | *RRMSE* | 6.25 | 5.87 |
| | *RMAE* | 4.39 | 4.22 |
| **Online sequential ELM (OSELM)** | *RRMSE* | 7.78 | 11.42 |
| | *RMAE* | 5.48 | 7.97 |
| **Extreme Learning Machine (ELM)** | *RRMSE* | 5.12 | 11.41 |
| | *RMAE* | 3.66 | 7.95 |
| **ICEEMDAN-RF** | *RRMSE* | 3.16 | 1.67 |
| | *RMAE* | 2.67 | 1.13 |
| **ICEEMDAN-OSELM** | *RRMSE* | 1.55 | 1.94 |
| | *RMAE* | 0.98 | 1.44 |
| **ICEEMDAN-ELM** | *RRMSE* | **1.51** | **1.50** |
| | *RMAE* | **0.93** | **0.96** |

reduces the modeling time which is of the essence when the forecast horizon is very short such as half-hourly in this study. Additionally, the ELM model is able to surmount the efficiency and scalability issues as ELM is highly efficient due to random allocation of input weights [83,84] with fewer manual tuning parameters since the network parameters are automatically generated [83,85]. ELM exhibits fast learning speed by concurrently avoiding the issues of learning rates, learning epochs, stopping criteria, and local optima [48,83] that were tedious and time-consuming approaches in traditional neural network models. The integration of computationally efficient ICEEMDAN decomposition technique with the ELM, which has the efficient running capability with reduced computational complexity, makes the hybrid ICEEMDAN-ELM well-suited for efficient very short-time forecasting and real-time applications [86–88]. Subsequently, the ICEEMDAN-ELM requires trivial human intervention and can further be explored in very short-time forecasting applications of other variables such as wind energy and solar radiation as long as the data sets are suitable.

Despite the enhanced performance of the newly developed ICEEMDAN-ELM model, some limitations of the present undertaking could be explored in further studies. This study utilized a single input variable approach, however, the Hs is contingent upon many climatic and oceanographic driving factors such as wind, solar radiation, sea surface temperature [26,79,89–92] and bathymetry. A comprehensive study with inclusion of these factors and others in forecasting of half-hourly effective wave height would provide more information on the physical characteristics of ocean waves and the performance of machine learning models.

The proposed collaborative ICEEMDAN-ELM model could be optimized by an ensemble modeling method (with confidence intervals of the Hs simulations) to possibly achieves more accurate results. An ensemble of model simulations could lead to a more strategic decision-making model, with the provisions of how accurate simulated Hs could be, in terms of the uncertainties between several forecasted data. Other advanced optimization methods that could be applied includes Quantum-Behaved PSO and Firefly Algorithm to select training inputs prior to being channeled into the ICEEMDAN-ELM model [93–101]. Further, empirical wavelet transform [102] and singular value decomposition [103] could be another avenue of this work. A future work could apply copula functions [104] as statistical tools where the joint behavior of multivariate data *e.g.*, Hs and corresponding predictors, can be modeled for any tested station.

In the current study, the ICEEMDAN-ELM model is applied for the purpose of very short-term Hs forecasting *i.e.*, half-hourly forecast horizon. It should be noted that for the purpose of strategic planning and management of energy production, there is a need for medium-term (that extends from 1 to 2 years into the future) to long-term (that extends beyond by many years such as 10-year projection or 30-year projections, *etc.)* Hs forecasts. Further independent research studies, at these forecast horizons, are also recommended.

## 6. Conclusion

In this study, an ICEEMDAN-ELM model is developed using the Hs data for training purposes as the predictors for the model forecasting of future Hs at Gold Coast and Mooloolaba stations. The Hs data from January-2000 to March-2018 at 30-min intervals were used to decompose into IMFs and residuals through ICEEMDAN algorithm. The PACF of the corresponding IMFs and residuals were computed where the significant lags were inserted into the ELM model to develop the ICEEMDAN-ELM model in order to achieve a high level of accuracy. For comparison, ICEEMDAN-OSELM, ICEEMDAN-RF, standalone ELM, OSELM, and RF models were used in this study. Several types of evaluation criterion were adopted to judge the accuracy of the proposed ICEEMDAN-ELM model.

As evident by low relative forecasting errors and high performance metrics, the performance of the ICEEMDAN-ELM model is somewhat better than those of counterpart models. The forecasting errors registered at both the sites from the ICEEMDAN-ELM were $RMSE \approx 0.016$ m (Gold Coast), 0.018 m (Mooloolaba), whereas the *MAE* was 0.010 m (Gold Coast), 0.012 m (Mooloolaba) respectively. In terms of the normalized performance metrics, the values of these metrics for both the stations from the ICEEMDAN-ELM model were $r \approx 0.999$, $WI \approx 0.999$ and $E_{NS} \approx 0.999$ (See; Tables 6 and 7).

The performance of the ICEEMDAN-ELM is assessed in relation to the comparative models using Legates-McCabe's index. The obtained *LM* agreement values between the forecasted and observed Hs for the Gold Coast site was $LM \approx 0.969$ from the proposed ICEEMDAN-ELM model. The relative percentage errors *RRMSE* and *RMAE* were only 1.51%, 0.93% (ICEEMDAN-ELM) compared to 1.55%, 0.98% (ICEEMDAN-OSELM), 3.16%, 2.67% (ICEEMDAN-RF), 5.12%, 3.66% (ELM), 7.78%, 5.58% (OSELM) and 6.25%, 4.39% (RF). A reasonable degree of geographic variability was evident on the basis of relative percentage errors *RRMSE* and *RMAE* with the optimal performance acquired for Gold Coast site on the basis of *RRMSE* as compared to Mooloolaba site in the accuracy of the ICEEMDAN-ELM model being followed.

This study provides a baseline in terms of historical half-hourly Hs data, being utilized to forecast future Hs values. Incorporation of other climatological parameters and bathymetry data could be explored in future studies. Forecast of Hs at medium to long-term forecast horizons could enable the government and impacted stakeholders in strategic future renewable energy and coastal planning. Moreover, the proposed ICEEMDAN-ELM model could also be applied to other areas such as solar radiation and electricity demand forecasting that would assist the policymakers in the optimal management of energy generation resources.

## Acknowledgements

The significant wave height data was acquired from Environment and Science, Queensland Government, Coastal Data System, Queensland, Australia and the authors are thankful for that. We also duly acknowledge that this research project has been sponsored by The University of Southern Queensland's Postgraduate Research Scholarship (2017–2019) awarded to both the authors, managed by the Office of Research and Graduate Studies Division. The authors are also grateful to both the reviewers in providing constructive feedback in improving the quality of the paper.

## References

[1] Thies PR, Johanning L, Gordelier T. Component reliability testing for wave energy converters-rationale and implementation. In: Proceedings of the European wave and tidal energy conference. Aalborg, Denmark; 2013.

[2] CSIRO. Ocean renewable energy: 2015–2050. An analysis of ocean energy in Australia. Energy transformed and wealth from oceans flagships. CSIRO; 2012.
[3] Reikard G. Forecasting ocean wave energy: tests of time-series models. Ocean Eng 2009;36:348–56.
[4] Duan W-Y, Huang L-M. A hybrid EMD-AR model for nonlinear and non-stationary wave forecasting. J Zhejiang Univ Sci A 2016;17:115–29.
[5] Özger M, Altunkaynak A, Şen Z. Statistical investigation of expected wave energy and its reliability. Energy Convers Manag 2004;45:2173–85.
[6] Mahjoobi J, Etemad-Shahidi A. An alternative approach for the prediction of significant wave heights based on classification and regression trees. Appl Ocean Res 2008;30:172–7.
[7] Etemad-Shahidi A, Mahjoobi J. Comparison between M5′ model tree and neural networks for prediction of significant wave height in Lake Superior. Ocean Eng 2009;36:1175–81.
[8] Berbić J, Ocvirk E, Carević D, Lončar G. Application of neural networks and support vector machine for significant wave height prediction. Oceanologia 2017;59:331–49.
[9] Malekmohamadi I, Bazargan-Lari MR, Kerachian R, Nikoo MR, Fallahnia M. Evaluating the efficacy of SVMs, BNs, ANNs, and ANFIS in wave height prediction. Ocean Eng 2011;38:487–97.
[10] Kazeminezhad MH, Etemad-Shahidi A, Mousavi SJ. Application of fuzzy inference system in the prediction of wave parameters. Ocean Eng 2005;32:1709–25.
[11] Cuadra L, Salcedo-Sanz S, Nieto-Borge JC, Alexandre E, Rodríguez G. Computational intelligence in wave energy: comprehensive review and case study. Renew Sustain Energy Rev 2016;58:1223–46.
[12] Adamowski J, Fung Chan H, Prasher SO, Ozga-Zielinski B, Sliusarieva A. Comparison of multiple linear and nonlinear regression, autoregressive integrated moving average, artificial neural network, and wavelet artificial neural network methods for urban water demand forecasting in Montreal, Canada. Water Resour Res 2012:48.
[13] Adamowski J, Chan HF. A wavelet neural network conjunction model for groundwater level forecasting. J Hydrol 2011;407:28–40.
[14] Wang D, Wei S, Luo H, Yue C, Grunder O. A novel hybrid model for air quality index forecasting based on two-phase decomposition technique and modified extreme learning machine. Sci Total Environ 2017;580:719–33.
[15] Deo RC, Tiwari MK, Adamowski JF, Quilty MJ. Forecasting effective drought index using a wavelet extreme learning machine (W-ELM) model. Stoch Environ Res Risk Assess 2017;31:1211–40.
[16] Le Maıtre O, Najm HN, Ghanem R, Knio O. Multi-resolution analysis of Wiener-type uncertainty propagation schemes. J Comput Phys 2004;197:502–31.
[17] Kim B-G, Shim J-I, Park D-J. Fast image segmentation based on multi-resolution analysis and wavelets. Pattern Recognit Lett 2003;24:2995–3006.
[18] Mallat SG. A theory for multiresolution signal decomposition: the wavelet representation. IEEE Trans Pattern Anal Mach Intell 1989;11:674–93.
[19] Nourani V, Hosseini Baghanam A, Adamowski J, Kisi O. Applications of hybrid wavelet–Artificial Intelligence models in hydrology: a review. J Hydrol 2014;514:358–77.
[20] Tiwari M, Adamowski J, Adamowski K. Water demand forecasting using extreme learning machines. J Water Land Dev 2016:28.
[21] Krishna B, Rao YRS, Nayak PC. Time series modeling of river flow using wavelet neural networks. J Water Resour Prot 2011;03:50–9.
[22] Deka PC, Prahlada R. Discrete wavelet neural network approach in significant wave height forecasting for multistep lead time. Ocean Eng 2012;43:32–42.
[23] Prahlada R, Deka PC. Forecasting of time series significant wave height using wavelet decomposed neural network. Aquat Procedia 2015;4:540–7.
[24] Dixit P, Londhe S. Prediction of extreme wave heights using neuro wavelet technique. Appl Ocean Res 2016;58:241–52.
[25] Dixit P, Londhe S, Dandawate Y. Removing prediction lag in wave height forecasting using Neuro-Wavelet modeling technique. Ocean Eng 2015;93:74–83.
[26] Özger M. Significant wave height forecasting using wavelet fuzzy logic approach. Ocean Eng 2010;37:1443–51.
[27] Rathinasamy M, Khosa R, Adamowski J, ch S, Partheepan G, Anand J, et al. Wavelet-based multiscale performance analysis: an approach to assess and improve hydrological models. Water Resour Res 2014;50:9721–37.
[28] Prasad R, Deo RC, Li Y, Maraseni T. Input selection and performance optimization of ANN-based streamflow forecasts in the drought-prone Murray Darling Basin region using IIS and MODWT algorithm. Atmos Res 2017;197:42–63.
[29] Cornish CR, Bretherton S, Percival DB. Maximal overlap wavelet statistical analysis with application to atmospheric turbulence. Netherlands: Kluwer Academic Publishers; 2005.
[30] Dghais AAA, Ismail MT. A comparative study between discrete wavelet transform and maximal overlap discrete wavelet transform for testing stationarity. Int J Math Comput, Phys Electr Comput Eng 2013;12:1677–81.
[31] Percival DB, Lennox SM, Wang YG, Darnell RE. Wavelet-based multiresolution analysis of Wivenhoe Dam water temperatures. Water Resour Res 2011:47.
[32] Chen J, Heincke B, Jegen M, Moorkamp M. Using empirical mode decomposition to process marine magnetotelluric data. Geophys J Int 2012;190:293–309.
[33] Huang NE, Shen Z, Long SR, Wu MC, Shih HH, Zheng Q, et al. The empirical mode decomposition and the Hilbert spectrum for nonlinear and non-stationary time series analysis. Proc R Soc 1998;A 454:903–95.
[34] Wu Z, Huang NE, Wallace JM, Smoliak BV, Chen X. On the time-varying trend in global-mean surface temperature. Clim Dyn 2011;37:759–73.
[35] Duan WY, Han Y, Huang LM, Zhao BB, Wang MH. A hybrid EMD-SVR model for the short-term prediction of significant wave height. Ocean Eng 2016;124:54–73.
[36] Wu Z, Huang NE. Ensemble empirical mode decomposition: a noise-assisted data analysis method. Adv Adapt Data Anal 2009;1:1–41.
[37] Torres ME, Colominas MA, Schlotthauer G, Flandrin P. A complete ensemble empirical mode decomposition with adaptive noise. In: Proceedings of the 2011 IEEE international conference on acoustics, speech and signal processing (ICASSP); 2011. p. 4144–7.
[38] Colominas MA, Schlotthauer G, Torres ME. Improved complete ensemble EMD: a suitable tool for biomedical signal processing. Biomed Signal Process Control 2014;14:19–29.
[39] Han H, Cho S, Kwon S, Cho S-B. Fault diagnosis using improved complete ensemble empirical mode decomposition with adaptive noise and power-based intrinsic mode function selection algorithm. Electronics 2018:7.
[40] Rabah A, Abdelhafid K. Rolling bearing fault diagnosis based on improved complete ensemble empirical mode of decomposition with adaptive noise combined with minimum entropy deconvolution. J Vibroeng. 2018;20:240–57.
[41] Olvera-Guerrero OA, Prieto-Guerrero A, Espinosa-Paredes G. Decay Ratio estimation in BWRs based on the improved complete ensemble empirical mode decomposition with adaptive noise. Ann Nucl Energy 2017;102:280–96.
[42] Li X, Li C. Pretreatment and wavelength selection method for near-infrared spectra signal based on improved CEEMDAN energy entropy and permutation entropy. Entropy 2017:19.
[43] Li X, Li C. Improved CEEMDAN and PSO-SVR modeling for near-infrared non-invasive glucose detection. Comput Math Methods Med 2016;2016:8301962.
[44] Al-Musaylh MS, Deo RC, Li Y, Adamowski JF. Two-phase particle swarm optimized-support vector regression hybrid model integrated with improved empirical mode decomposition with adaptive noise for multiple-horizon electricity demand forecasting. Appl Energy 2018;217:422–39.
[45] Kumar NK, Savitha R, Al Mamun A. Ocean wave height prediction using an ensemble of Extreme Learning Machine. Neurocomputing 2018;277:12–20.
[46] Cornejo-Bueno L, Nieto-Borge JC, García-Díaz P, Rodríguez G, Salcedo-Sanz S. Significant wave height and energy flux prediction for marine energy applications: a grouping genetic algorithm – extreme learning machine approach. Renew Energy 2016;97:380–9.
[47] Huang NE, et al. Shen Z, Long SR, Wu MC, Shih HH, Zheng Q. The empirical mode decomposition and the Hilbert spectrum for nonlinear and non-stationary time series analysis. Proc R Soc Lond A: Math Phys Eng Sci: R Soc 1998:903–95.
[48] Huang G-B, Zhu Q-Y, Siew C-K. Extreme learning machine: a new learning scheme of feedforward neural networks. In: Proceedings of the IEEE international joint conference on neural networks (IEEE Cat No04CH37541) 2004; 2004. p. 985–90.
[49] Rajesh R, Prakash JS. Extreme learning machines-a review and state-of-the-art. Int J Wisdom Based Comput 2011;1:35–49.
[50] Huang G-B. What are extreme learning machines? filling the gap between Frank Rosenblatt's Dream and John von Neumann's puzzle. Cognit Comput 2015;7:263–78.
[51] Tamura Si, Tateishi M. Capabilities of a four-layered feedforward neural network: four layers versus three. IEEE Trans Neural Netw 1997;8:251–5.
[52] Huang G-B. Learning capability and storage capacity of two-hidden-layer feedforward networks. IEEE Trans Neural Netw 2003;14:274–81.
[53] Liang N-Y, Huang G-B, Saratchandran P, Sundararajan N. A fast and accurate online sequential learning algorithm for feedforward networks. IEEE Trans Neural Netw 2006;17:1411–23.
[54] Lan Y, Soh YC, Huang G-B. Ensemble of online sequential extreme learning machine. Neurocomputing 2009;72:3391–5.
[55] Yadav B, Ch S, Mathur S, Adamowski J. Discharge forecasting using an online sequential extreme learning machine (OS-ELM) model: a case study in Neckar River, Germany. Measurement 2016;92:433–45.
[56] Schapire RE, Freund Y, Bartlett P, Lee WS. Boosting the margin: a new explanation for the effectiveness of voting methods. Ann Stat 1998:1651–86.
[57] Breiman L. Bagging predictors. Mach Learn 1996;24:123–40.
[58] Breiman L. Random forests. Mach Learn 2001;45:5–32.
[59] Robert B, Yoav F, Peter B, Sun LW. Boosting the margin: a new explanation for the effectiveness of voting methods. Ann Stat 1998;26:1651–86.
[60] Segal MR. Machine learning benchmarks and random forest regression. 2004.
[61] Liaw A, Wiener M. Classification and regression by random forest. R News 2002;2:18–22.
[62] Queensland. Environment and Science; 2018.
[63] ABS. Australian Bureau of Statistics; 2016.
[64] Hemer MA, Zieger S, Durrant T, O'Grady J, Hoeke RK, McInnes KL, et al. A revised assessment of Australia's national wave energy resource. Renew Energy 2017;114:85–107.
[65] Kim T-W, Valdes JB. Nonlinear model for drought forecasting based on a conjunction of wavelet transforms and neural networks. J Hydrol Eng 2003;8:319–28.
[66] Deo RC, Tiwari MK, Adamowski JF, Quilty JM. Forecasting effective drought index using a wavelet extreme learning machine (W-ELM) model. Stoch Environ Res Risk Assess 2016.
[67] Ren Y, Suganthan PN, Srikanth N. A comparative study of empirical mode decomposition-based short-term wind speed forecasting methods. IEEE Trans Sustain Energy 2015;6:236–44.
[68] Ouyang Q, Lu W, Xin X, Zhang Y, Cheng W, Yu T. Monthly rainfall forecasting using EEMD-SVR based on phase-space reconstruction. Water Resour Manag 2016;30:2311–25.
[69] Wang W-C, Xu D-M, Chau K-W, Chen S. Improved annual rainfall-runoff forecasting using PSO–SVM model based on EEMD. J Hydroinform 2013;15:1377–90.
[70] Hsu C-W, Chang C-C, Lin C-J. A practical guide to support vector classification. 2003.
[71] Yen BC. Discussion and closure: criteria for evaluation of watershed models. J Irrig Drain Eng 1995;121:130–2.
[72] Dawson CW, Abrahart RJ, See LM. HydroTest: a web-based toolbox of evaluation

metrics for the standardised assessment of hydrological forecasts. Environ Model Softw 2007;22:1034–52.
[73] Deo RC, Wen X, Qi F. A wavelet-coupled support vector machine model for forecasting global incident solar radiation using limited meteorological dataset. Appl Energy 2016;168:568–93.
[74] Legates DR, McCabe GJ. Evaluating the use of "goodness-of-fit" Measures in hydrologic and hydroclimatic model validation. Water Resour Res 1999;35:233–41.
[75] Willmott CJ. Some comments on the evaluation of model performance. Bull Am Meteorol Soc 1982;63:1309–13.
[76] Willmott CJ. On the validation of models. Phys Geogr 1981;2:184–94.
[77] Willmott CJ. On the evaluation of model performance in physical geography. Spatial statistics and models. Springer; 1984. p. 443–60.
[78] Foresee FD, Hagan MT. Gauss-Newton approximation to Bayesian learning. Neural networks, 1997, In: Proceedings of the international conference on: IEEE. 1997. p. 1930–5.
[79] Reikard G, Robertson B, Bidlot J-R. Wave energy worldwide: simulating wave farms, forecasting, and calculating reserves. Int J Mar Energy 2017;17:156–85.
[80] Gonçalves M, Martinho P, Guedes Soares C. Wave energy conditions in the western French coast. Renew Energy 2014;62:155–63.
[81] Bequé A, Lessmann S. Extreme learning machines for credit scoring: an empirical evaluation. Expert Syst Appl 2017;86:42–53.
[82] Prasad R, Deo RC, Li Y, Maraseni T. Soil moisture forecasting by a hybrid machine learning technique: ELM integrated with ensemble empirical mode decomposition. Geoderma 2018;330:136–61.
[83] Albadr MAA, Tiun S. Extreme learning machine: a review. Int J Appl Eng Res 2017;12:4610–23.
[84] Chen X, Dong ZY, Meng K, Xu Y, Wong KP, Ngan HW. Electricity price forecasting with extreme learning machine and bootstrapping. IEEE Trans Power Syst 2012;27:2055–62.
[85] Şahin M, Kaya Y, Uyar M, Yıldırım S. Application of extreme learning machine for estimating solar radiation from satellite data. Int J Energy Res 2014;38:205–12.
[86] Huang G, Huang GB, Song S, You K. Trends in extreme learning machines: a review. Neural Netw 2015;61:32–48.
[87] Frances-Villora JV, Rosado-Muñoz A, Martínez-Villena JM, Bataller-Mompean M, Guerrero JF, Wegrzyn M. Hardware implementation of real-time extreme learning machine in FPGA: analysis of precision, resource occupation and performance. Comput Electr Eng 2016;51:139–56.
[88] Deo RC, Downs N, Parisi AV, Adamowski JF, Quilty JM. Very short-term reactive forecasting of the solar ultraviolet index using an extreme learning machine integrated with the solar zenith angle. Environ Res 2017;155:141–66.
[89] Uihlein A, Magagna D. Wave and tidal current energy – a review of the current state of research beyond technology. Renew Sustain Energy Rev 2016;58:1070–81.
[90] Gunn K, Stock-Williams C. Quantifying the global wave power resource. Renew Energy 2012;44:296–304.
[91] Langhamer O, Haikonen K, Sundberg J. Wave power—sustainable energy or environmentally costly? A review with special emphasis on linear wave energy converters. Renew Sustain Energy Rev 2010;14:1329–35.
[92] Falcão AFdO. Wave energy utilization: a review of the technologies. Renew Sustain Energy Rev 2010;14:899–918.
[93] Hoang N-D, Pham A-D, Cao M-T. A novel time series prediction approach based on a hybridization of least squares support vector regression and swarm intelligence. Appl Comput Intell Soft Comput 2014;2014:15.
[94] Kayarvizhy N, Kanmani S, Uthariaraj R. ANN models optimized using swarm intelligence algorithms. WSEAS Trans Comput 2014;13:501–19.
[95] Kumar D, Prasad RK, Mathur S. Optimal design of an in-situ bioremediation system using support vector machine and particle swarm optimization. J Contam Hydrol 2013;151:105–16.
[96] Pal SK, Rai C, Singh AP. Comparative study of firefly algorithm and particle swarm optimization for noisy non-linear optimization problems. Int J Intell Syst Appl 2012;4:50.
[97] Sedki A, Ouazar D. Hybrid particle swarm and neural network approach for streamflow forecasting. Math Model Nat Phenom 2010;5:132–8.
[98] Taormina R, Chau K-W. Data-driven input variable selection for rainfall-runoff modeling using binary-coded particle swarm optimization and Extreme Learning Machines. J Hydrol 2015.
[99] Taormina R, Chau K-W, Sivakumar B. Neural network river forecasting through baseflow separation and binary-coded swarm optimization. J Hydrol 2015;529:1788–97.
[100] Raheli B, Aalami MT, El-Shafie A, Ghorbani MA, Deo RC. Uncertainty assessment of the multilayer perceptron (MLP) neural network model with implementation of the novel hybrid MLP-FFA method for prediction of biochemical oxygen demand and dissolved oxygen: a case study of Langat River. Environ Earth Sci 2017;76:503.
[101] Ghorbani MA, Deo Ravinesh C, Zaher Mundher Y, Mahsa HK, Babak M. Pan evaporation prediction using a hybrid multilayer perceptron-firefly algorithm (MLP-FFA) model: case study in North Iran. Theor Appl Climatol 2017.
[102] Gilles J. Empirical wavelet transform. IEEE Trans Signal Process 2013;61:3999–4010.
[103] Chau K, Wu C. A hybrid model coupled with singular spectrum analysis for daily rainfall prediction. J Hydroinform 2010;12:458–73.
[104] Nguyen-Huy T, Deo RC, An-Vo D-A, Mushtaq S, Khan S. Copula-statistical precipitation forecasting model in Australia's agro-ecological zones. Agric Water Manag 2017;191:153–72.